FISEVIER

Contents lists available at ScienceDirect

Resources, Conservation & Recycling

journal homepage: www.elsevier.com/locate/resconrec



Full length article

Zn leaching recovery and mechanisms from end-of-life tire rubber

Shiyu Li^a, Thien Q. Tran^b, Qi Li^a, Bin Ji^a, Alexander S. Brand^{b,c}, Wencai Zhang^a

- ^a Department of Mining and Minerals Engineering, Virginia Polytechnic Institute and State University, Blacksburg, VA 24061, USA
- b The Charles Edward Via, Jr. Department of Civil and Environmental Engineering, Virginia Polytechnic Institute and State University, Blacksburg, Virginia, 24060, USA
- ^c Department of Material Science and Engineering, Blacksburg, Virginia Polytechnic Institute and State University, Blacksburg, Virginia, 24060, USA

ARTICLE INFO

Keywords: Tire rubber Zinc Recovery Leaching Kinetics

ABSTRACT

Experiments were conducted to investigate the leaching behavior of Zn from end-of-life tire rubber. XRD and XPS analyses showed that the Zn-containing phase in the material was mainly ZnO. SEM-EDS analysis confirmed the presence of both exposed and encapsulated ZnO particles. Acid leaching tests indicated that the carbon black comprised in the material can be oxidized and dissolved by HNO $_3$, resulting in the dissolution of completely encapsulated ZnO particles with thinner covering layers. Then, leaching tests using HNO $_3$ as the lixiviant were performed by varying acid concentration and leaching temperature. The results showed over 98% of Zn can be recovered using 2.0 mol/L HNO $_3$ at 90 °C after 400 min of reaction. Leaching kinetic results were best fit with the Avrami model, indicating the leaching process was controlled by diffusion. The activation energy determined by Arrhenius formula was 12.92 kJ/mol, which further supports the proposed diffusion controlled leaching process.

1. Introduction

The increasing production of vehicles is responsible for the dynamic growth of automobile waste materials, mostly in the form of waste tires. Based on the latest reports, around 2.27 billion tonnes of tires were produced in 2021 around the world, and the generation of waste tires is estimated to be over 1 billion tonnes annually (Devani et al., 2022; Kole et al., 2017). Tires normally contain 40% to 60% rubber polymer, 20% to 35% reinforcing agents (e.g., carbon black), 15% to 20% aromatic extender oils, and 4% vulcanization additive (e.g., zinc oxide, benzothiazole, and derivatives) (Dall'Osto et al., 2014). The wide range of chemical compositions and the cross-linked structures of rubber in the tire make it challenging to be treated by biodegradation, chemicals, and high temperature (De et al., 2001). The accumulation of used tires, therefore, poses a serious threat to the environment.

Several processes have been reported to recycle waste tires aiming to reduce the waste volume and enhance the recycling performance. One of the most valuable waste tire applications is to convert to recycled products such as rubber mulch and rubber paves, which can be used for sidewalks, animal flooring, playground surfaces, *etc.* (Llompart et al., 2013; Tran et al., 2022). Gasification, pyrolysis, or plasma are commonly used for tire-to-energy conversion (Huang and Tang, 2007; Huang et al., 2007), and waste tire pyrolysis oil has been assessed on the combustion, emission, performance, and noise characteristics of

compression ignition engines, which is an effective technique for waste management and fossil fuel alternatives (Ağbulut et al., 2021; Karagöz et al., 2020). Moreover, the waste tire residue after fuel transformation can be regarded as a valuable byproduct for pollutant removal (Gupta et al., 2011). The activated carbon derived from waste tire rubber has enhanced surface area and pore volume, resulting in excellent adsorbent materials (Gupta et al., 2014; Mui et al., 2004).

In addition to the organic materials, some valuable metals, such as iron (Fe), copper (Cu), zinc (Zn), and cobalt (Co) are involved in the tire manufacturing process serving as stabilizers and additives (Kinoshita et al., 2005). Among these metals, the Zn content in the tire is considered the highest, which accounts for 1% to 2% of the tire by weight (Gunasekara et al., 2000; Liu et al., 2018; Rhodes et al., 2012). Zinc oxide (ZnO) has been generally used as the activator for sulfur vulcanization in the tire manufacturing industry (Thaptong et al., 2019). With the accumulation of waste tires, concerns have been raised regarding the toxic effects that Zn may have on human health and aquatic ecosystems (Chapman and Johnson, 2005). For example, it has been estimated that over 7000 tons of ZnO are generated from waste tires every year, which has been evaluated by toxicity identification as the common cause of poisoning to plants, and microorganisms (Nelson et al., 1994; Wik, 2007). Considering that Zn possesses unique physical, chemical, thermal, electrical, and isolating properties and is applied in many industrial sectors including automotive, aerospace, construction, electricity,

https://doi.org/10.1016/j.resconrec.2023.107004

^{*} Corresponding author.

E-mail address: jibin93@vt.edu (B. Ji).

energy, electronics, and mechanical engineering (Nilsson et al., 2017), recovering Zn from waste tires is worthwhile for both environmental protection and economic profit production.

The hydrometallurgical process is a widely applied method for metal recovery from low-grade and complex ores, which is usually easy-tooperate, economically feasible, and obtains satisfactory metal recoveries (Behnamfard et al., 2013; Ippolito et al., 2021). Actually, studies have reported the Zn recovery from tire-related materials using the hydrometallurgical method (Gregurek et al., 2015; Kinoshita et al., 2005; Rhodes et al., 2012), where mineral acids were applied as the lixiviants for the Zn leaching from waste tires or fly ash of waste tires, and the results showed that over 90% of Zn was recovered using 1.0 mol/L HNO $_3$ at 23 $^{\circ}\text{C}$ and Zn recovery increases with smaller crumb rubber and longer exposure time. Moreover, selective recovery of Zn from the leach liquor was achieved when solvent extraction was performed (Kinoshita et al., 2005). In some cases, a pretreatment method is required to improve the efficiency of the subsequent leaching process. More than 90% of Zn originally present in waste tire fly ash was recovered by water leaching after thermal treatment. By heating the mixture of fly ash of waste tire and polyvinyl chloride (PVC), the released hydrogen chloride (HCl) from PVC was adsorbed by the fly ash, thus converting the crystalline ZnO into chlorides. The water soluble zinc chloride (ZnCl2) was then recovered easily by water leaching (Yamaguchi et al., 2006). Therefore, the feasibility of Zn recovery from waste tires has been investigated, but there have been no studies focusing on the effects of acid types, acid concentrations, and temperatures on the recovery of Zn from waste tire rubber.

In this study, raw tire rubber particles were used as the feedstock to evaluate the leaching recovery of Zn. XRD, XPS, and SEM-EDS analyses were conducted to characterize the mineralogical features, chemical states, and morphological characteristics of Zn-containing particles. Then, the tire rubber particle was treated with different types of mineral acids to determine the lixiviant providing the optimal leaching behavior. The Zn recovery was further optimized using the selected acid by varying the acid concentration and leaching temperature. By analyzing the morphological changes of the tire rubber particle, the mechanism of Zn leaching recovery from tire rubber was determined. In addition, the leaching data was fitted with various kinetic models to evaluate the leaching performance. This study presents the association characteristics of ZnO as well as the leaching behavior of Zn from end-of-life tire rubber under various condition, which explains the leaching mechanism and provides novel aspects for the Zn recovery and utilization of waste tires.

2. Material and methods

2.1. Materials

Micronized tire rubber particle in the size range of $<400~\mu m$ was manufactured by Lehigh Technologies (Tucker, GA, USA). The free-flowing black particle with a specific gravity of $1.14\pm0.03~g/cm^3$ is produced from end-of-life tires that consist of natural rubber, butadiene rubber, and styrene-butadiene rubber, according to the manufacturer. The sample was used as received without any further treatments in this study.

The chemicals used In this study include hydrochloric acid (HCl, 37 wt.%), nitric acid (HNO $_3$, 67 wt.% to 70 wt.%), sulfuric acid (H $_2$ SO $_4$, 93 wt.% to 98 wt.%), and hydrofluoric acid (HF, 48 wt.% to 51 wt.%), which were all trace metal grade purchased from Thermo Fisher Scientific, USA. Type I deionized water used for all tests in this study was prepared by Direct-Q Water Purification System (Millipore, USA) with a resistivity of 18.2 M Ω cm at 25 °C.

2.2. Methods

2.2.1. Determination of Zn concentration in tire rubber particle

As a result of the chemical stability of tire rubber, it is challenging to digest or dissolve the whole material for the determination of total Zn concentration. In order to measure the Zn concentration accurately, the tire rubber was pretreated by a dry ashing method followed by digestion. Specifically, 5.0 g of the tire rubber was loaded into a porcelain crucible which was then placed in a muffle furnace (EW-33,858–80, Cole-Parmer, USA). The furnace was located inside a fume hood to safely vent any volatile gases. Ashing was performed at 600 °C until a constant weight was reached, and the sample was then cooled down to ambient temperature before being collected for digestion.

The ashed tire rubber was digested using a microwave digestion system (Multiwave GO Plus, Anton Paar, USA). Initially, around 0.1 g of sample, 12 mL aqua regia (3 mL HNO $_3$, 9 mL HCl), and 3 mL HF were added into a 100 mL polytetrafluoroethylene (PTFE) vessel. The vessel was then inserted into the digestion rotor, and the digestion temperature reached 185 °C after 10 min of heating and maintained pressure for 40 min. When the digestion temperature decreased to 70 °C, the compressed acid gas in the PTFE vessel was carefully released into a fume hood. The digestion solution was centrifuged, and the supernatant was diluted 1000 times with 5% (v/v) HNO $_3$. The Zn concentration in the supernatant was measured by an inductively coupled plasma emission mass spectrometer (ICP-MS, Thermo Electron iCAP-RQ, Thermo Scientific, USA). The Zn content (mg/kg) in the tire rubber particle was calculated based on the following equation:

$$Zn\ content = \frac{C \times V}{m} \times \frac{M}{5} \tag{1}$$

where C (mg/L) and V (L) represent the Zn concentration in the digestion solution and the digestion volume, respectively, m (kg) is the mass of ashed tire rubber used for digestion, and M (g) is the weight of dry ashing product, and 5 is the mass (g) used for dry ashing.

The concentrations of major metals (i.e., Mg, Al, Ca, and Fe) present in the tire rubber particle were also evaluated by the same method as that of Zn.

2.2.2. Acid leaching tests

The acid leaching reaction occurred in a three-necked round bottom flask of 500 mL maximum volumetric capacity. The flask was immersed into a temperature-controllable water bath, which was loaded on a magnetic stirrer to keep the temperature constant and thoroughly mix the slurry. A reflux condenser was attached to the flask to prevent water evaporation. Before conducting the systematical investigations, a series of preliminary tests were designed by the software Design-Expert to investigate the effect of various parameters on the Zn recovery. It was found that the solid concentration had negligible effect on the Zn recovery, therefore, it was kept constant in the following tests. Detailed analysis of the preliminary tests is included in the Supporting document.

First, three acids (HNO $_3$, HCl, and H $_2$ SO $_4$) were used to investigate the effect of acid types on the leaching characteristics of Zn from the material. For each test, 100 mL acid solution of 1 mol/L was preheated to 70 °C prior to the addition of 5.0 g sample, equating to a solid concentration of 50 g/L. The resultant mixture was agitated using a PTFE-coated magnetic stirrer at 600 rpm. After 400 min of reaction, the slurry was filtered using 2.5 μ m pore size filter paper. The filtrate was collected and diluted 100 times with 5% (v/v) HNO $_3$ for ICP-MS analysis.

By comparing the leaching performance, the most efficient acid that can provide the highest recovery value was identified. To further optimize the leaching conditions, two series of experiments were conducted to investigate the effect of acid concentration and leaching temperature on the Zn recovery from the tire rubber using the most efficient acid. The first series of experiments were conducted using 0.5 mol/L, 1.0 mol/L,

and 2.0 mol/L acid solution as the lixiviant, while the acid concentration of the second series was set constant at 2.0 mol/L acid solution with the leaching temperature varying from 25 °C to 90 °C (i.e., 25 °C, 50 °C, 70 °C, and 90 °C). The other leaching conditions were the same as those mentioned above. During the leaching process, representation samples of 2 mL were collected from the slurry to evaluate the leaching characteristics of Zn at various time intervals from the start of the reaction up to a total period of 400 min (i.e., 5 min, 10 min, 20 min, 30 min, 60 min, 120 min, 200 min, 300 min, and 400 min). Upon collection, solid-liquid separation of the samples was immediately achieved by centrifugation. The Zn concentration was measured by ICP-MS after the liquid fraction was diluted 100 times with 5% (v/v) HNO3, which was then used to calculate the leaching recovery of Zn from the tire rubber. After the reaction, the remaining slurry was filtered, and the filter cake was thoroughly rinsed with deionized water. The leaching residue was then dried at 60 °C overnight for further characterization.

2.3. Characterization

The X-ray diffraction (XRD) analysis of the materials was conducted by a Bruker D8 Advance Twin diffractometer employing Ni-filtered Cu-K α radiation source. Patterns were recorded with an operating voltage of 40 kV and current of 40 mA, in a 20 scanning range of 10–70° with a scan speed of 2° per min. The peaks were indexed using MDI Jade 6.5 software, with PDF-2 database from International Center for Diffraction Data (ICDD).

X-ray photoelectron spectroscopy (XPS) was carried out to investigate the surface chemistry of the composites, which was performed on PHI Quantera SXM equipped with a scanning monochromatic X-ray source (Al-K $\alpha=1486.7$ eV). The average depth of analysis for an XPS measurement is approximately 5 nm. The samples were mounted on non-conductive adhesive tape and placed in the instrument. All the samples were analyzed at an electron take-off angle of 45°, and the results were analyzed by PHI MultiPak V9.0 software.

The morphology and microstructure of the samples were characterized by a JSM-IT500 scanning electron microscope (SEM) equipped with backscattered electron (BSE) systems. The samples were mounted on conductive carbon adhesive holders and sputtered with palladium/platinum (10 nm thickness) to increase their electron conductivity. To identify and locate Zn-containing particles associated with the rubber particle, energy dispersive spectroscopy (EDS) elemental mapping was first conducted on the specimens with Zn being selected as the predetermined element. If a brighter region is noticed, then the elemental composition of the region will be analyzed using EDS point-mode at various accelerating voltages.

The obtained SEM images were processed by ImageJ software to evaluate the particle size changes of the tire rubber samples. ImageJ is a public domain Java image processing software (Collins, 2007; Hörenz et al., 2020). After acquiring high-quality SEM images, scale calibration and binary conversion were conducted. The particles were segregated and their boundaries from the background and from each other were determined. For each sample, around 100 grains were selected for particle size analysis, and the average values were reported in the result. The detailed measurement descriptions can be found in published studies (Mazzoli and Favoni, 2012; Vladár and Hodoroaba, 2020).

A Quantachrome Autosorb-1 analyzer was used to measure the Brunauer-Emmett-Teller (BET) surface area and porous volume of the samples, which connected with ultra-high-purity grade $\rm N_2$, He, and $\rm CO_2$ gases. Prior to the adsorption analysis, all the samples were evacuated under a dynamic vacuum overnight at 80 °C. $\rm N_2$ adsorption isotherm measurements were performed at liquid nitrogen temperature. The surface area was determined at the relative pressure range of 0.05 < equilibrium pressure (kPa)/saturation pressure (kPa) (P/P0) < 0.30, and the volume of $\rm N_2$ adsorbed at the relative pressure of 0.99 was used to calculate the total pore volume of the sample.

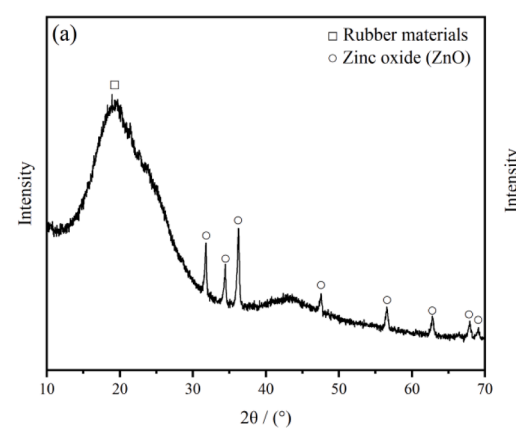
3. Results and discussion

3.1. Sample characterization

The mineralogical features of the tire rubber particle were characterized by XRD analysis, and the XRD pattern is shown in Fig. 1(a). The most intensive peak at 2θ of around 20° indicates a broad amorphous scattering hump, which corresponds to rubber materials, such as natural rubber, acrylonitrile butadiene rubber, and styrene-butadiene-styrene (Johns and Rao, 2008; Singh and Varma, 2012; Tahir et al., 2015). Several sharp peaks of zinc oxide (ZnO) were found in the pattern, indicating that ZnO was the major metal oxide compound present in the tire rubber particles. Considering the detection limits of XRD analysis, XPS characterization was performed to further analyze the surface chemistry of the tire rubber particle. As shown in Fig. 1(b), the survey scan revealed the presence of Zn and inorganic materials like Si in the tire rubber particle. The peak shown in the inset at a binding energy of around 1021.80 eV was assigned to $\text{Zn } 2p_{3/2}$ peak of Zn^{2+} , which can be originated from oxide (Choi et al., 2016; Jing et al., 2001). In addition, a weak peak located at around 163.2 eV was attributed to the S 2p photoelectron peak. It has been reported that the S 2p peak resulted from the S²⁻ in the zinc sulfide (ZnS) structure or the surface defects of the S-S species in the ZnS shell layer (Liang and Wang, 2018; Zhou et al., 2016). Actually, the vulcanization process of the tire industry promotes the formation of a trace amount of nano-sized ZnS that are highly dispersed within the carbonaceous matrix, and several studies have confirmed the existence of ZnS in the tire rubber (Sun et al., 2022; Wang et al., 2021). A combined analysis of the XRD and XPS results indicated that the dominant Zn-containing phase in the tire rubber was ZnO, while the remaining occurred as ZnS. Table 1 indicates the concentrations of major metals in the tire rubber particle. Based on the ICP-MS analysis, it is shown that the material contained over 10,000 mg/kg of Zn, which is much higher than the content of other metals. This conclusion was also corroborated by the XRD and XPS analyses that the Zn-containing phases were the only detectable metal compound present in the tire rubber particle. The high content of Zn suggested that the material is a promising feedstock for Zn recovery.

SEM characterization was performed on the tire rubber particles to evaluate their morphology and surface characteristics. As shown in Fig. 2(a), the particles had irregular and angular shapes with a maximum dimension of around 0.5 mm. Observations of the particles under higher magnification (e.g., Fig. 2(b)) showed that the particle surfaces are smooth with negligible microcracks and pores, indicating a relatively low surface area of the tire rubber particle. This finding is consistent with studies on tire wastes obtained from the cryogenic destruction process (Fazli and Rodrigue, 2020; Yerezhep et al., 2021). Zn-containing particles were found on the surface of the tire rubber particles, and based on the EDS analysis, it was inferred that the Zn existed in the form of ZnO (Fig. 2(c)(d)). The ZnO particle exposed on the surface had a dimension of less than 100 μ m, and was closely associated with the tire rubber.

In addition, ZnO particles encapsulated within the tire rubber were also found using SEM-EDS. As Fig. 2(e)(h) shows, three bright regions, referred to as Z1, Z2, and Z3, respectively, corresponded to ZnO particles when using 20 kV as the accelerating voltage. When the voltage decreased to 10 kV (Fig. 2(f)(i)), Z1 and Z2 regions were still bright, while no noticeable difference in brightness was observed between the Z3 region and the overall image. However, as shown in Fig. 2(g)(j), further decreasing the voltage to 5 kV, the Zn-enriched particles cannot be detected and no bright regions were observed. The gradual decline of brightness from 20 kV to 5 kV can be explained by the decrease in backscattered electron energies, which results in the reduction of electron penetration depth as well as the poor efficiency of the elemental imaging (Isabell and Dravid, 1997). This phenomenon indicates that the ZnO particles were completely encapsulated by the tire rubber with different thicknesses of encapsulating layer. By analyzing the SEM-EDS



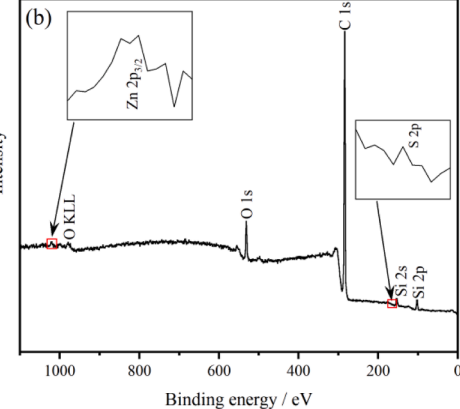


Fig. 1. XRD pattern (a) and full range XPS spectra (b) of the raw tire rubber particle (Note: Zn 2p_{3/2} and S 2p electronic peaks are presented at inset.).

Table 1Concentrations of major metals in the tire rubber particle.

Metal	Mg	Al	Ca	Fe	Zn
mg/kg	566.5	218.9	627.0	130.6	10,389.2

result, it can be concluded that both the exposed and encapsulated ZnO particles exist in the tire rubber particles. However, as a result of the dispersal characteristics and trace amount of the nano-sized particles, ZnS particles were not found in the specimens under SEM-EDS analysis. Therefore, ZnO was selected as the targeting Zn-containing phase within the tire rubber particle in the following discussion.

3.2. Acid selection for Zn leaching

To determine the most promising mineral acid for Zn recovery from the tire rubber particle, leaching experiments were carried out using different types of acids (i.e., HCl, HNO3, and $\rm H_2SO_4$) as the lixiviants with the acid concentration being fixed at 1.0 mol/L. The leaching temperature was kept constant at 70 °C, and the leaching reaction lasted for 400 min. Fig. 3 shows the effect of acid types on the leaching recovery of Zn from the tire rubber particle, it can be seen that less than 10% of Zn was extracted from the material after 400 min of reaction when using 1.0 mol/L HCl, and under the same leaching conditions, the recovery value was slightly increased using 1.0 mol/L $\rm H_2SO_4$. However, the Zn recovery value reached over 30% when 1.0 mol/L HNO3 was employed as the lixiviant, which is much higher than the recoveries obtained with HCl and $\rm H_2SO_4$.

It is well known that rubber materials have good resistance to acid attacks even after being immersed in 5% to $10\%~H_2SO_4$ solutions for several days (Rahimi et al., 2016; Thomas and Gupta, 2016). However, the carbon black comprised in the tire rubber can be oxidized and dissolved by HNO $_3$, resulting in the presence of crevasses, slit-shaped pores, broken carbon layers, and hollow cell structure (Kamegawa et al., 1998; Norwitz and Galan, 1967). It was also noted that a reddish-brown NO $_2$ gas was liberated during the leaching process, and the reaction can be written by the following equation:

$$C(s) + 4HNO_3(l) = CO_2(g) + 2H_2O(l) + 4NO_2(g)$$
 (2)

As indicated by the SEM-EDS analysis in Section 3.1, there are two encapsulation types of ZnO particles present in the tire rubber particle: partially encapsulated particles and completely encapsulated particles with various covering thicknesses. The partially encapsulated ZnO particles can be dissolved during the acid-leaching process, while it is difficult for the completely encapsulated particles to be exposed to the acid solutions as a result of the covering layer. However, the cracks and dissolution of carbon black resulted from HNO₃ oxidization exposed the

encapsulated ZnO particles, which provide the possibility for the extraction of ZnO particles by HNO_3 solution. The morphology of the leaching residue of the samples treated with different types of acid was examined by SEM analysis shown in Fig. 4. Compared with the raw tire rubber particle (Fig. 2(a)(b)), minimal difference in morphology was observed from the samples after being leached by 1.0 mol/L HCl and H_2SO_4 solutions. While cavities and flaws were observed on the surface of the sample treated by 1.0 mol/L HNO3, some particles even had rough surfaces and deep cracks (Fig. 4(c)(d)). It can be inferred that the completely encapsulated ZnO particles with thinner covering layers will be first leached as the gradual oxidization and cracking of carbon black by HNO3 treatment, leading to a relatively higher Zn recovery. Therefore, HNO3 was determined as the most effective lixiviant which deserved further optimization to realize desired Zn recovery.

3.3. HNO3 leaching

3.3.1. Effect of acid concentration

The effect of HNO₃ concentration on the leaching characteristics of Zn was studied in the concentration range of 0.5 mol/L to 2.0 mol/L at 70 °C while maintaining other conditions constant. As observed from Fig. 5, around 5% of Zn was extracted from the tire rubber particle within the first 5 min of reaction when 0.5 mol/L HNO₃ was employed as the lixiviant, and only minimal recovery gains (≈3 percentage points) were obtained by prolonging the reaction time to 400 min. By increasing the HNO3 concentration to 1.0 mol/L, the recovery curve almost overlapped with that of the 0.5 mol/L HNO₃ within the first 30 min; after that, the leaching recovery increased, and a final value of 26% was obtained after the completion of the reaction. It is worth mentioning that a sudden increase in recovery was observed between 30 min to 120 min, while the increasing trend was relatively flat after that. When using 1.0 mol/L HNO₃ as the lixiviant, more cracks were expected to form on the surface of the particles as a result of a strongly oxidizing environment. As the leaching reaction progressed, the completely encapsulated ZnO particles with thinner covering layers were exposed first, and the dissolution of these exposed particles resulted in a sudden increase in Zn recovery. However, a stronger oxidizing condition was required to obtain higher recoveries by exposing the completely encapsulated ZnO particles with thicker covering layers. Further elevating the HNO3 concentration to 2.0 mol/L as shown, a negligible difference in Zn recovery can be noticed within the first 10 min relative to that of 0.5 mol/L and 1.0 mol/L HNO3. However, after the first 10 min, the leaching recovery of Zn increased gradually and reached over 60% after the completion of the reaction. This result indicated that more completely encapsulated ZnO particles can be exposed in a stronger oxidizing condition, thus resulting in higher recovery values.

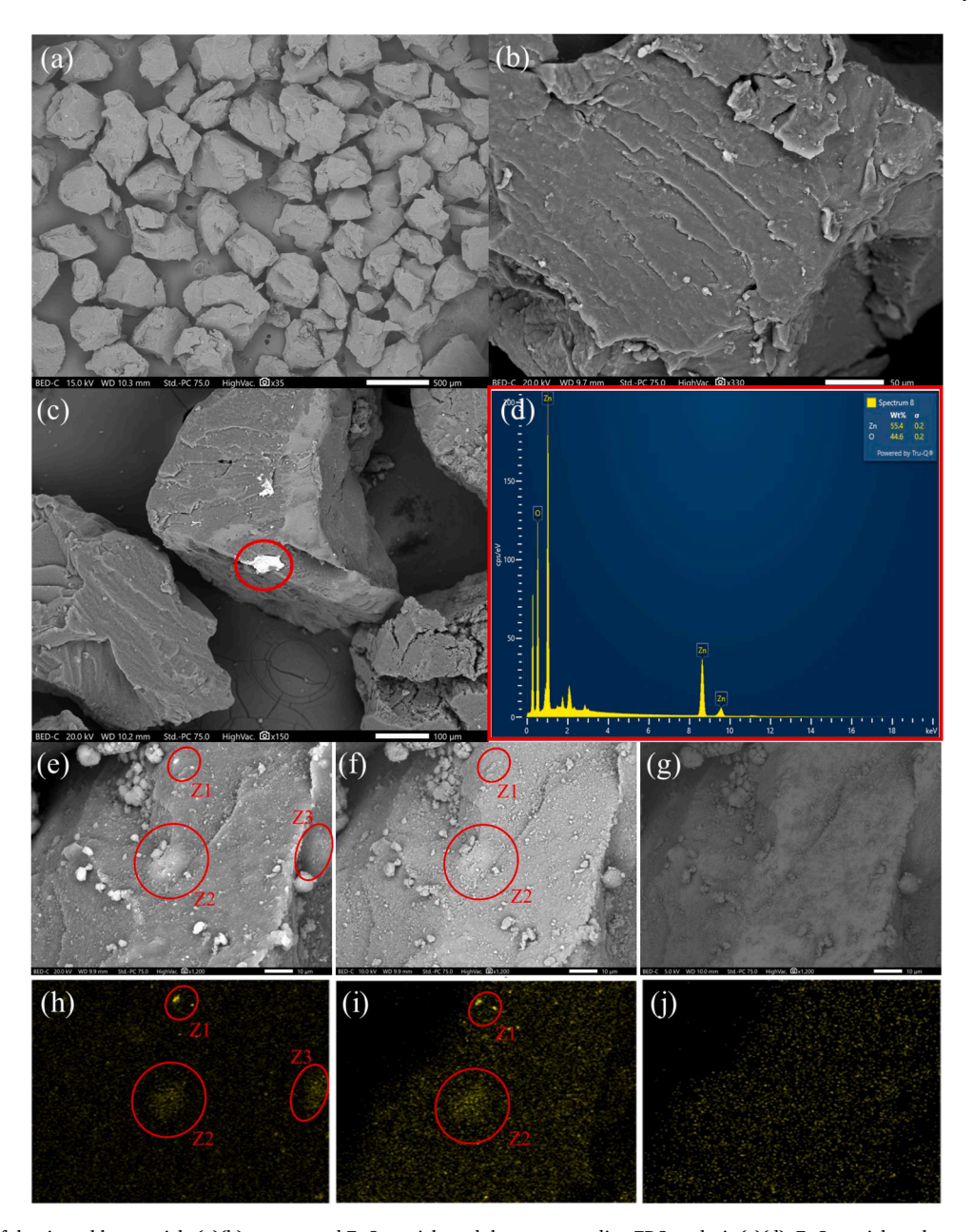


Fig. 2. SEM images of the tire rubber particle (a)(b), an exposed ZnO particle and the corresponding EDS analysis (c)(d), ZnO particles taken at different accelerating voltages and the corresponding EDS mapping of Zn: (e)(h) 20 kV, (f)(i) 10 kV, and (g)(j) 5 kV. (The ZnO particle is marked with red circles.).

3.3.2. Effect of leaching temperature

Acid leaching tests were performed to study the effect of leaching temperature on the leaching characteristics of Zn from tire rubber particles. The lixiviant used in this investigation was 2.0 mol/L HNO₃, and the leaching temperatures were 25 °C, 50 °C, 70 °C, and 90 °C, while the other leaching parameters remained constant. The result is presented in Fig. 6.

It can be observed that the leaching recovery of Zn increased with increasing temperature. For example, around 5% of Zn was released at 25 $^{\circ}\text{C}$ after 400 min of reaction, which means that the completely encapsulated ZnO particles cannot be sufficiently exposed at low temperatures even in a strongly oxidizing environment. When the sample was treated with 2.0 mol/L HNO3 at 50 $^{\circ}\text{C}$, the leaching recovery of Zn reached over 17% within the first 60 min of reaction and increased to 25% after 400 min of leaching. The relatively lower leaching kinetics after the first 60 min of reaction indicated that the leaching conditions were insufficient to further oxidize the tire rubber particles and could

not expose more completely encapsulated ZnO particles. When increasing the leaching temperature to 70 °C, the Zn recovery increased to over 35% within the first 120 min of reaction, and the leaching kinetics was faster than that obtained at 50 °C (~20% recovery). After that, the leaching recovery increased gradually with the proceeding of the leaching reaction and reached a final recovery value of around 60%. Moreover, contrasting the slow leaching kinetics observed at 25 °C and 50 °C after the first 120 min of reaction, the leaching recovery increased by 24 absolute percentage points from 120 to 400 min of reaction at 70 °C, which indicates higher temperature enables further oxidization of the particles and exposes more ZnO particles, thus leading to higher leaching recoveries. Raising the leaching temperature to 90 °C, the final leaching recovery of Zn increased significantly to over 98%, which means almost all the Zn-containing particles were leached after the completion of the reaction. This result demonstrated that nearly all the completely encapsulated particles can be exposed when using 2.0 mol/L HNO₃ as the lixiviant at 90 °C.

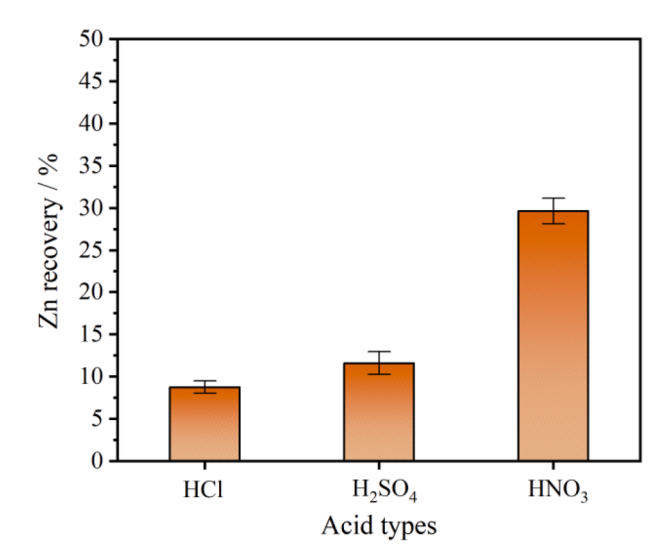


Fig. 3. The effect of acid types on the leaching recovery of Zn from tire rubber particles (1 mol/L acid concentration, $70\,^{\circ}$ C leaching temperature, $50\,$ g/L solid concentration, and $400\,$ min leaching duration).

After the acid leaching tests under various temperatures, the solid residue was collected and subjected to SEM analysis for morphological characterization. As shown in Fig. 7, the leaching residue obtained at 25 °C had sharp edges, smooth surface, and negligible microcracks and pores, suggesting a similar morphology to that of the raw tire rubber particles (Fig. 2(a)). This result indicated that the 25 °C leaching temperature cannot expose the ZnO particles encapsulated within the tire rubber, which explained the extremely low recovery values obtained at this temperature (Fig. 6). Fig. 7(b)(c) exhibits the morphology of the residue obtained from the leaching test with 2.0 mol/L HNO $_3$ at 50 °C, minor differences were observed in the overall morphology relative to that of the 25 °C leaching residue. However, some cracks and micropores

were present in the SEM image of higher magnification as a result of the oxidization of carbon black (Fig. 7(c)), which enabled the dissolution of ZnO particles encapsulated by thinner covering layers, thus leading to a higher leaching recovery value than the leaching test at 25 $^{\circ}$ C. Fig. 7(d) shows the morphology of the leaching residue after 60 min of reaction at 70 $^{\circ}$ C, which is similar to that of the final leaching residue obtained at 50 $^{\circ}$ C (Fig. 7(b)).

As the reaction proceeded at 70 $^{\circ}$ C, the leaching recovery of Zn increased gradually and reached around 40% at 200 min of reaction (Fig. 6). The leaching residue after 200 min of reaction at 70 $^{\circ}$ C was collected and characterized by SEM, and some white flake particles were observed on a cracked tire rubber particle in the form of inclusion.

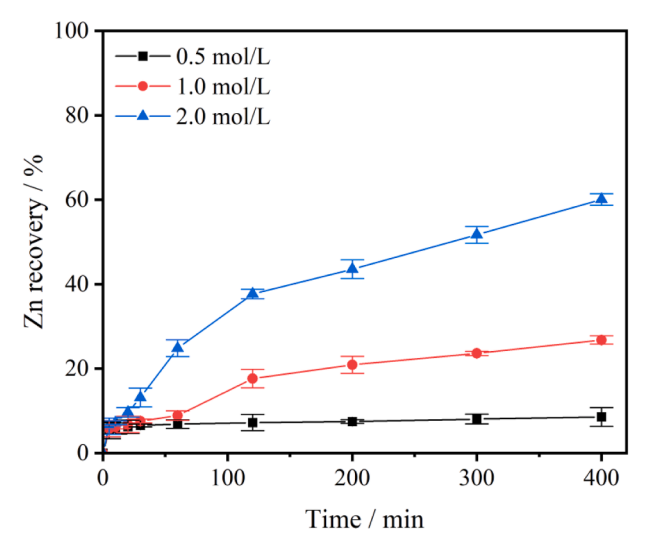


Fig. 5. Effect of acid concentration on the leaching characteristics of Zn from the tire rubber particle (HNO $_3$ as the lixiviant, 70 $^{\circ}$ C leaching temperature, 50 g/L solid concentration, and 400 min leaching duration).

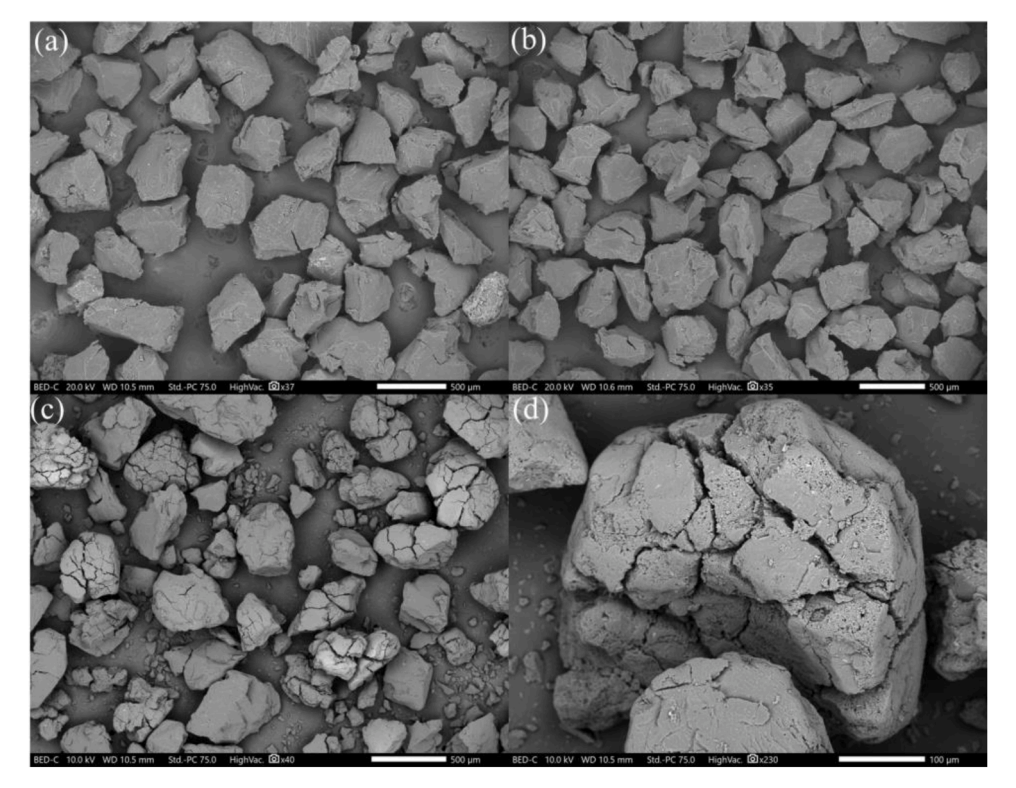


Fig. 4. SEM images of the leaching residue of tire rubber particle treated by different types of acid: (a) HCl, (b) H₂SO₄, and (c)(d) HNO₃.

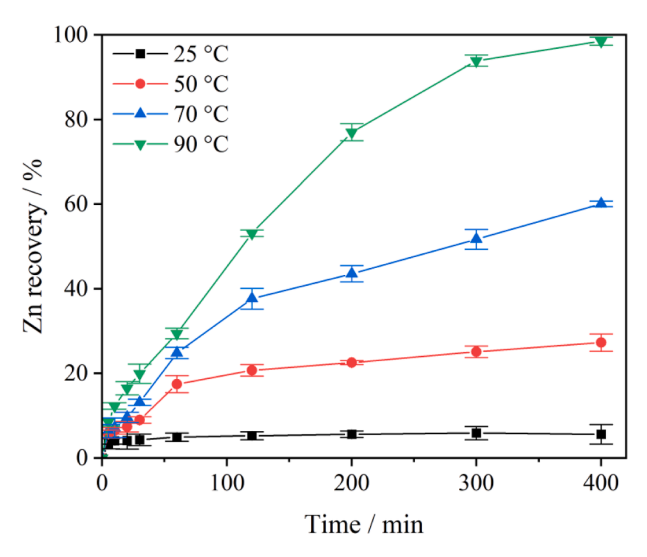


Fig. 6. Effect of leaching temperature on the leaching characteristics of Zn from tire rubber particle (2.0 mol/L HNO_3 as the lixiviant, 50 g/L solid concentration, and 400 min leaching duration).

Elemental maps as well as EDS spectra (Figure S1 in the supporting document) confirmed that these flake white particles were ZnO particles. These results indicated that the further oxidization and dissolution of carbon black led to deep cracks in the particles as the reaction continued at 70 °C, which exposed more encapsulated ZnO particles. The exposed ZnO particles were then dissolved in HNO₃ solution, which led to the further improvement of Zn recovery. After 400 min of reaction at 90 °C, almost all the ZnO particles were leached. The morphology of

the final leaching residue is presented in Fig. 7(g)-(i). As shown, more obvious cracks appeared in the particles, and some particles even broke up as a result of the oxidization of carbon black and the dissolution of ZnO. In addition, it is interesting to note that some holes with a diameter of around 50 μm were observed in the tire rubber particles, which is the evidence of the complete dissolution of encapsulated ZnO particles. Under higher leaching temperature, more cracks and holes were formed on the surface of the tire rubber, which exposed the encapsulated ZnO particles, thus leading to the significantly improved recovery. This result was in accordance with the findings of the preliminary tests (see in Supporting document).

In order to investigate the effect of leaching temperature on the textual properties of the tire rubber, N_2 adsorption measurements were conducted on the final leaching residue of the samples leached at different temperatures. In addition, the changes in particle size of the representative samples at various time intervals (i.e., 60 min, 200 min, and 400 min) were also examined. Fig. 8 shows the N_2 adsorption isotherms and corresponding pore size distributions, as well as the changes in particle size of the samples, while the weight loss after the leaching reaction and the textual properties are summarized in Table 2.

After being leached by 2.0 mol/L HNO $_3$ at 25 °C for 400 min, the leaching residue exhibited a negligible N $_2$ adsorbed volume over a series of high relative pressure, and the corresponding curve was a typical Type II isotherm according to the IUPAC classification (Sing et al., 1985), which suggests the sample had low specific surface area and total pore volume (Table 2). Compared with the 25 °C leaching residue, the leaching residue of 50 °C showed a similar isotherm, but with a relatively larger specific surface area (7.80 m 2 /g) and total pore volume (0.0105 cm 3 /g). The pore size distribution analysis showed certain increases in the proportion of pores in the 3 nm to 10 nm range. In addition, the particle size of the 50 °C leaching residue decreased

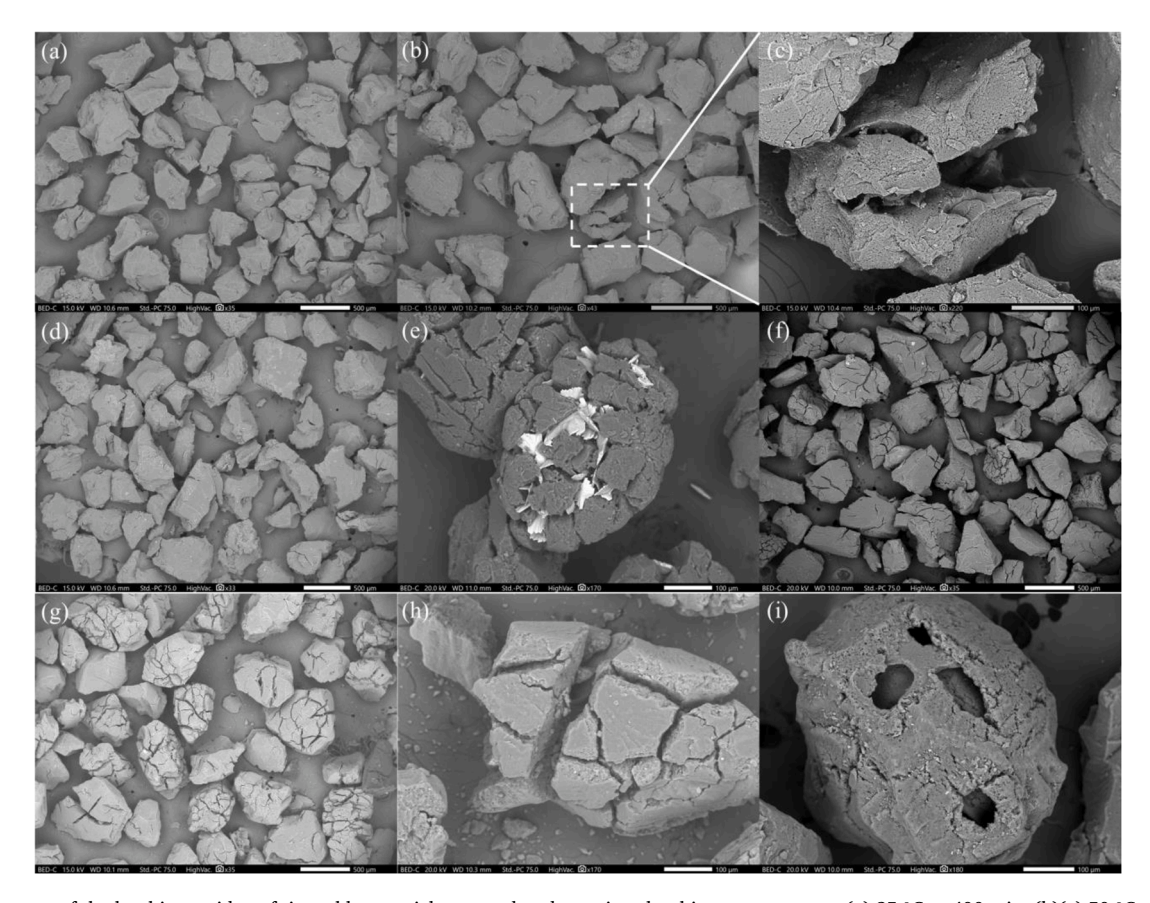


Fig. 7. SEM images of the leaching residue of tire rubber particles treated under various leaching temperatures: (a) 25 °C at 400 min, (b)(c) 50 °C at 400 min, (d) 70 °C at 60 min, (e) 70 °C at 200 min, (f) 70 °C at 400 min, and (g)-(i) 90 °C at 400 min.

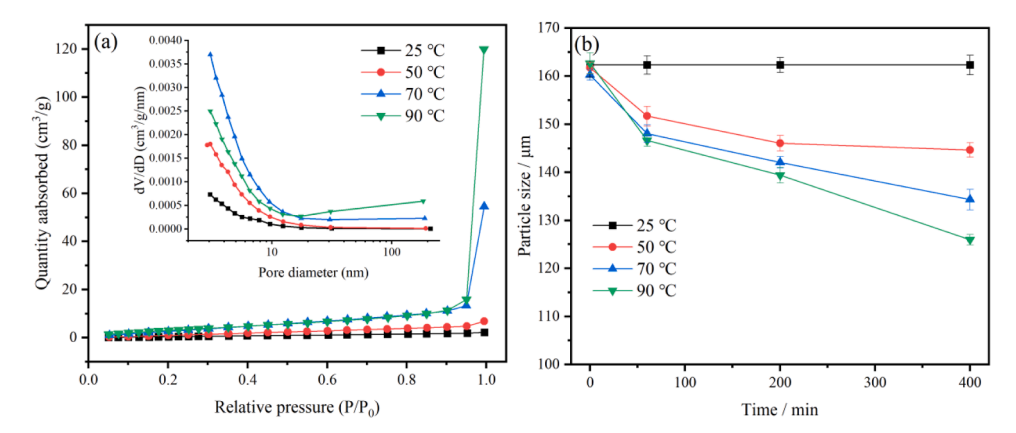


Fig. 8. (a) N₂ adsorption isotherms and the corresponding pore size distribution curves (inset), and (b) particle size changes of the tire rubber particle treated by 2.0 mol/L HNO₃ at various temperatures.

Table 2 Weight loss and textural properties of the tire rubber particle treated by 2.0 mol/L $\rm HNO_3$ at various temperatures.

Leaching temperature	Weight loss (%)	$S_{BET}^{a} (m^2/g)$	V _{tot} ^b (cm ³ /g)	D _{avg} ^c (nm)
25 °C	0.59	3.27	0.0034	2.61
50 °C	1.46	7.80	0.0105	7.92
70 °C	13.12	15.56	0.0843	63.74
90 °C	21.08	28.39	0.1855	140.22

^a S_{BET}: BET specific surface area;.

noticeably from 161 μm to 151 μm within the first 60 min, and the decreasing trend tended to be flat afterward. This result indicated that pores and cracks were formed on the surface of the tire rubber particles, and the dissolution of carbon black was confirmed by the particle size reduction, which means some completely encapsulated ZnO particles with a thinner covering layer can be exposed. Those exposed particles were then leached under acidic conditions, leading to the Zn recovery increases observed in Fig. 6. Elevating the leaching temperature to 70 °C caused a weight loss of 13.1% (Table 2), and the particle size decreased gradually to 135 µm after the completion of the reaction. Moreover, the relatively higher adsorbed volume of N2 suggested a larger specific surface area (15.56 m²/g), total pore volume (0.0843 cm³/g), and average pore diameter (63.74 nm) compared with that of the 25 °C and 50 °C leaching residues. The residue of the 90 °C leaching test showed the highest adsorbed volume of N₂ and possessed the largest proportion of pores bigger than 20 µm (Fig. 8(a)). Meanwhile, the final particle size decreased significantly to less than 130 µm with a weight loss of 21.08%. Combined with the leaching results shown in Fig. 6, it can be inferred that the carbon black was further dissolved, and all the completely encapsulated ZnO particles regardless of the covering layer thickness were exposed and leached at 90 °C with 2.0 mol/L HNO3. The cracking and dissolution of the tire rubber particles as well as the leaching of ZnO particles resulted in pores with larger diameters. This phenomenon was corroborated by the highest values of specific surface area $(28.39 \text{ m}^2/\text{g})$, total pore volume (0.1885 cm³/g), and average pore diameter (63.74 nm).

In this study, over 98% of Zn can be recovered at 90 °C when using 2.0 mol/L HNO3 as the lixiviant, which indicates a promising resource recovery from the end-of-life tire rubber. However, if only taking the leaching process into consideration, the cost incurred and waste liquid generated are not economically feasible. The primary focus of the current study is to further purify the Zn from the leachate, and reuse the recovered Zn in the production of new tires. In addition, the leaching residue will be evaluated in the infrastructure applications such as soil

additives, and aggregates in portland cement and asphalt concretes (Tran et al., 2022). The comprehensive utilization as well as the huge stockpiles of waste tires will definitely offset the cost, and improve the economic viability of the recycling process.

3.4. Leaching kinetics

The leaching process of tire rubber particles is a reaction between the liquid and solid, which can be treated as a heterogeneous reaction expressed by the following equation:

$$A (liquid) + B (solid) \rightarrow Products$$
 (3)

In order to make a better understanding of the interaction mechanisms, the leaching recovery values versus time at various temperatures (Fig. 6) were analyzed and correlated with different types of kinetic models. Comprehensive information regarding the rate controlling step of Zn leaching process was obtained from the analysis and correlation. If a surface chemical reaction occurs slowly, the shrinking core model can be used to describe the dissolution kinetics by Eq. (4) (Amiri et al., 2012; Levenspiel, 1998);

$$1 - (1 - X)^{\frac{1}{3}} = K_a t \tag{4}$$

Similarly, if rate-controlling step governs the diffusion of the reagent through the product layer, Eq. (5) is suitable for the description of the dissolution kinetics (Ajibove et al., 2019):

$$1 - 3(1 - X)^{\frac{2}{3}} + 2(1 - X) = K_b t \tag{5}$$

If reaction rate is controlled by both the interface transfer and diffusion across the product layer, Eq. (6) is sufficient to explain the Zn leaching process (Dickinson and Heal, 1999; Wadsworth Sec and Miller, 1979).

$$1/3 \ln(1-X) - \left[1 - (1-X)^{\frac{-1}{3}}\right] = K_c t$$
 (6)

In addition to the three models mentioned above, a model suggested by Avrami was developed originally from the crystallization phenomenon and has been successfully applied to explain the leaching kinetic data of non-catalytic fluid-solid reactions (Demirkiran and Künkül, 2007; Tunç et al., 2007; Zhang et al., 2011, 2015). The Avrami model and the corresponding logarithm form are expressed as follows:

$$-\ln(1-X) = K_d t^n \tag{7}$$

$$\ln(-\ln(1-X)) = \ln K_d + n\ln t \tag{8}$$

In Eqs. 4–8, X represents the leaching recovery value, t means the reaction time (min), and K_{a_1} K_{b_2} , K_{c_3} , and K_{d_4} are apparent reaction constants. In the case of the Avrami model, n is the order of the reaction and

^b V_{tot} : total pore volume at P/P₀=0.99;.

 $^{^{}c}$ D_{avg} : average pore diameter.

does not change with leaching conditions. When n < 0.5, the reaction is governed by the diffusion process; when 0.5 < n < 1, the leaching reaction is controlled by both chemical reaction control and diffusion control; when n = 1, the initial reaction rate is finite, and the chemical reaction dominates the leaching process; while when n > 1, the initial reaction rate is approaching to zero (Gu et al., 2019; Lin et al., 2018).

The fitting curves of various kinetic models are shown in Fig. 9, and the liner fitting parameters are listed in Table 3. As shown, for the different leaching temperatures, a good linear relationship was observed between $\ln(-\ln(1-X))$ and $\ln t$ with the correlation coefficients (R²) all over 0.99, indicating the leaching process of Zn from the tire rubber particles fits well with the Avrami model. In spite of the leaching temperatures, n values of the four lines were less than 0.5, revealing that the mechanism of Zn leaching from the particles was controlled by diffusion. The $\mathrm{Zn^{2+}}$ was dissolved and diffused into the solution when using 2.0 mol/L HNO3 as the lixiviant under various temperatures. While the higher leaching temperature promoted the diffusion of H^+ and NO3¯into the tire rubber particle, which oxidized and dissolved the carbon black. Therefore, the encapsulated Zn-containing particles were exposed, thus leading to the recovery of Zn from the material.

The relationship between reaction constant K and temperature can be calculated by the Arrhenius formula:

$$K = Ae^{\frac{-Ea}{RT}}$$
 or $\ln K = -\frac{E_a}{RT} + \ln A$ (9)

where K presents the reaction constant, A indicates the frequency factor, E_a (kJ/mol) is the reaction activation energy, R means the ideal gas constant, and T is the absolute temperature. By plotting $\ln K$ against 1/T based on the Arrhenius formula, the values of reaction activation energy (E_a) and frequency factor (A) can be determined from the slope and intercept of the fitting curve as shown in Fig. 10. The activation energy (E_a) and frequency factor (A) calculated from the Arrhenius formula are

Table 3Fitting results of the selected kinetic models.

T / °C	Kinetic expression	Regression equation	R^2
	1/2	. 1/2	
25	$1-(1-X)^{1/3} = K_1t$	$1-(1-X)^{1/3} = 2E-05t+0.0141$	0.7170
	$1-3(1-X)^{2/3} + 2(1-X) =$	$1-3(1-X)^{2/3} + 2(1-X) = 2E$	0.7524
	K ₃ t	06t+0.0006	
	$1/3\ln(1-X) - [1-(1-X)^{-1/2}]$	$1/3\ln(1-X) - [1-(1-X)^{-1/3}] = 3E$	0.7539
	3] = $K_{2}t$	07t+0.0001	
	$ \ln\left[-\ln\left(1-X\right)\right] = \ln K + $	$ \ln\left[-\ln\left(1-X\right)\right] = $	0.9918
	nlnt	-4.1937+0.1254lnt	
50	$1 - (1 - X)^{1/3} = K_1 t$	$1-(1-X)^{1/3} = 0.0002t + 0.0302$	0.8379
	$1-3(1-X)^{2/3} + 2(1-X) =$	$1-3(1-X)^{2/3} + 2(1-X) = 7E$	0.9258
	K ₃ t	05t+0.0027	0.0400
	$1/3\ln(1-X) - [1-(1-X)^{-1/2}]$	$1/3\ln(1-X) - [1-(1-X)^{-1/3}] = 1E$	0.9403
	3] = $K_{2}t$	05t+0.0005	0.0064
	$ \ln\left[-\ln\left(1-X\right)\right] = \ln K + $	$\ln \left[-\ln (1 - X) \right] =$	0.9964
70	nInt	-3.9334+0.2245lnt $1-(1-X)^{1/3} = 0.0006$ t $+0.0343$	0.0500
70	$1-(1-X)^{1/3} = K_1t$ $1-3(1-X)^{2/3} + 2(1-X) =$	$1-(1-X)^{3/3} = 0.0006t+0.0343$ $1-3(1-X)^{2/3} + 2(1-X) = 0.0004t-$	0.9529 0.9848
	. , , , , ,	$1-3(1-X)^{-1} + 2(1-X) = 0.00041$ 0.0015	0.9848
	K ₃ t 1/3ln(1-X) – [1–(1-X ^{)–1/}	$1/3\ln(1-X) - [1-(1-X)^{-1/3}] =$	0.9822
	$\frac{1}{3}$ = $\frac{1}{1}$ = $\frac{1}{1}$	$1/3\ln(1-x) - [1-(1-x^2)] = 0.0001t - 0.0022$	0.9822
	$ \int_{0}^{\infty} = K_{2}t $ $ \ln \left[-\ln (1 - X)\right] = \ln K + $	ln [-ln (1 - X)] =	0.9972
		-3.6245+0.3608lnt	0.9972
90	$1-(1-X)^{1/3} = K_1t$	-3.0243+0.3008111 $1-(1-X)^{1/3} = 0.0018t+0.0296$	0.9840
90	$1-(1-X) = K_1t$ $1-3(1-X)^{2/3} + 2(1-X) =$	$1-3(1-X)^{2/3} + 2(1-X) = 0.0022t$	0.9840
	K_3t	0.0558	0.5//3
	$1/3\ln(1-X) - [1-(1-X)^{-1/2}]$	$1/3\ln(1-X) - [1-(1-X)^{-1/3}] =$	0.7943
	3 l = K ₂ t	0.0034t-0.1663	0.7 573
	$ \ln \left[-\ln \left(1 - X \right) \right] = \ln K + $	$\ln \left[-\ln (1 - X) \right] =$	0.9941
	$\lim_{t\to\infty} (1-x) = \lim_{t\to\infty} +$	-3.2471+0.4544lnt	0.7771
	111111	0.2 1/ 1 0. 10 1 Milt	

12.92 kJ/mol and 2.60 min⁻¹, respectively. The low activation energy also confirms that the leaching of Zn from tire rubber particles is a diffusion-controlled process (Ekmekyapar et al., 2012; Seyed Ghasemi

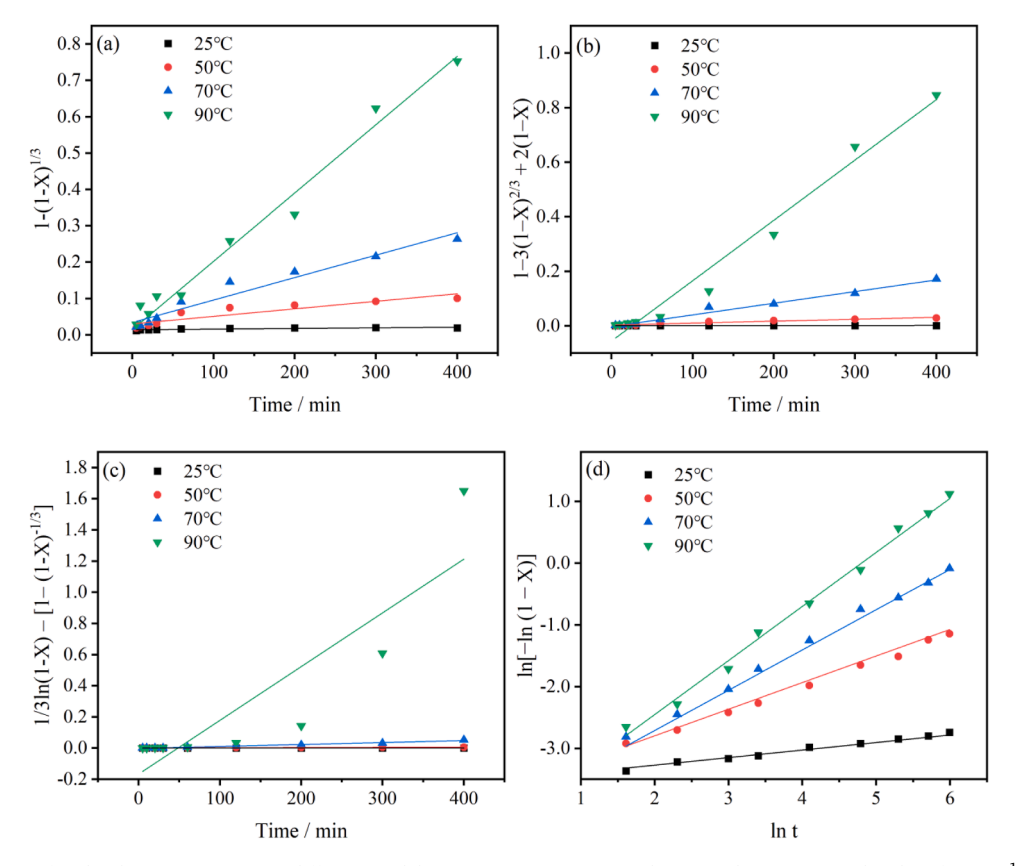


Fig. 9. The fitting curves of Zn leaching recovery using different models at temperature 25–90 °C by 2.0 mol/L HNO₃: (a) the plot of 1-(1-X)^{1/3} versus time, (b) the plot of $1-3(1-X)^{2/3} + 2(1-X)$ versus time, (c) the plot of $1/3\ln(1-X) - [1-(1-X)^{-1/3}]$ versus time, and (d) the plot of $\ln[-\ln(1-X)]$ versus lnt.

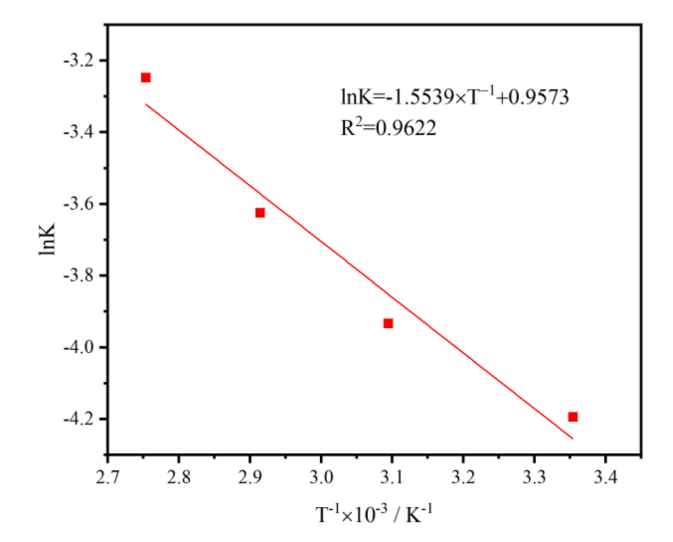


Fig. 10. Arrhenius plot for the leaching of Zn from tire rubber particles using 2.0 mol/L $\rm HNO_3$ under various temperatures.

and Azizi, 2018), which is in accordance with the leaching kinetic results. Therefore, a combined analysis of the leaching kinetic and thermodynamic results indicate that the diffusion process governs the Zn leaching from tire rubber particles using 2.0 mol/L $\rm HNO_3$ under various temperatures.

4. Conclusions

In the present study, tire rubber particles were used as the feedstock for Zn recovery. The XRD result showed that the ZnO was the only detectable metal compound present in the tire rubber particle, and the Zn content reached over 10,000 mg/kg. The morphological and surface characteristics were examined by SEM-EDS analysis. The result indicated that there were two types of ZnO particles associated with tire rubber particles, i.e., partially encapsulated particles, and completely encapsulated particles with various covering thicknesses. Acid leaching tests were first performed using HCl, H2SO4, and HNO3 to identify the most promising lixiviant for Zn recovery from tire rubber particles. Around 10% of Zn was recovered when using HCl and H2SO4 as the lixiviant, while the value for HNO3 was over 30% under the same leaching conditions. The morphology of the leaching residue was evaluated by SEM analysis, and it was found that the cracks and dissolution of carbon black resulted from HNO3 oxidization exposed to the encapsulated ZnO particles, which provide the possibility for the extraction of ZnO particles by HNO₃ solution.

Furthermore, the leaching behavior of Zn was examined by varying the HNO $_3$ concentrations (0.5–2.0 mol/L) and leaching temperatures (25 °C to 90 °C). The highest recovery value was obtained when using 2.0 mol/L HNO $_3$ as the lixiviant after 400 min of reaction at 90 °C. The samples treated under various temperatures were examined by SEM, BET, and particle size analyses. The results indicated that further oxidization and dissolution of carbon black as a result of the higher leaching temperature led to the exposure of the completely encapsulated ZnO particles, thus resulting in higher Zn recovery. The leaching recovery data were fitted by various kinetic models, and the Avrami model accurately reflected the leaching kinetic profiles of Zn from tire rubber particles. A combined analysis of leaching kinetic and thermodynamic results showed that the Zn leaching was governed by the diffusion process.

CRediT authorship contribution statement

Shiyu Li: Methodology, Data curation, Writing – original draft. **Thien Q. Tran:** Methodology, Data curation, Writing – review & editing.

Qi Li: Writing – review & editing. **Bin Ji:** Conceptualization, Writing – review & editing. **Alexander S. Brand:** Conceptualization, Supervision. **Wencai Zhang:** Conceptualization, Supervision, Validation.

Declaration of Competing Interest

Alex Brand, Wencai Zhang reports financial support was provided by Center for Tire Research.

Data availability

No data was used for the research described in the article.

Acknowledgements

This study was funded through the Center for Tire Research, Project SUST-2021-D14-4. The authors acknowledge Lehigh Technologies for providing the waste tire rubber.

Supplementary materials

Supplementary material associated with this article can be found, in the online version, at doi:10.1016/j.resconrec.2023.107004.

References

Ağbulut, Ü., Yeşilyurt, M.K., Sarıdemir, S., 2021. Wastes to energy: improving the poor properties of waste tire pyrolysis oil with waste cooking oil methyl ester and waste fusel alcohol – A detailed assessment on the combustion, emission, and performance characteristics of a CI engine. Energy 222, 119942. https://doi.org/10.1016/J. ENERGY.2021.119942.

Ajiboye, E.A., Panda, P.K., Adebayo, A.O., Ajayi, O.O., Tripathy, B.C., Ghosh, M.K., Basu, S., 2019. Leaching kinetics of Cu, Ni and Zn from waste silica rich integrated circuits using mild nitric acid. Hydrometallurgy 188, 161–168. https://doi.org/ 10.1016/J.HYDROMET.2019.06.016.

Amiri, F., Mousavi, S.M., Yaghmaei, S., Barati, M., 2012. Bioleaching kinetics of a spent refinery catalyst using Aspergillus niger at optimal conditions. Biochem. Eng. J. 67, 208–217. https://doi.org/10.1016/J.BEJ.2012.06.011.

Behnamfard, A., Salarirad, M.M., Veglio, F., 2013. Process development for recovery of copper and precious metals from waste printed circuit boards with emphasize on palladium and gold leaching and precipitation. Waste Manag. 33, 2354–2363. https://doi.org/10.1016/J.WASMAN.2013.07.017.

Chapman, A., Johnson, T., 2005. The role of zinc in the vulcanisation of styrenebutadiene rubbers. KGK Kautschuk Gummi Kunststoffe.

Choi, Y.I., Lee, S., Kim, S.K., Kim, Y.Il, Cho, D.W., Khan, M.M., Sohn, Y., 2016.
Fabrication of ZnO, ZnS, Ag-ZnS, and Au-ZnS microspheres for photocatalytic activities, CO oxidation and 2-hydroxyterephthalic acid synthesis. J. Alloys Compd. 675, 46–56. https://doi.org/10.1016/j.jallcom.2016.03.070.

Collins, T.J., 2007. ImageJ for microscopy. BioTechniques 43, S25–S30. https://doi.org/ 10.2144/000112517/ASSET/IMAGES/LARGE/FIGURE4.JPEG.

Dall'Osto, M., Beddows, D.C.S., Gietl, J.K., Olatunbosun, O.A., Yang, X., Harrison, R.M., 2014. Characteristics of tyre dust in polluted air: studies by single particle mass spectrometry (ATOFMS). Atmos. Environ. 94, 224–230. https://doi.org/10.1016/j. atmoseny.2014.05.026.

De, S.K., Sadhan, K., White, J.R., 2001. Rubber Technologist's Handbook, 576. Rapra Technology Limited.

Demirkiran, N., Künkül, A., 2007. Dissolution kinetics of ulexite in perchloric acid solutions. Int. J. Miner. Process. 83, 76–80. https://doi.org/10.1016/J. MINPRO.2007.04.007.

Devani, V., Umam, M.I.H., Aiza, Y., Sarbaini, S., 2022. Optimization of tire production planning using the goal programming method and sensitivity analysis. Int. J. Comput. Sci. Appl. Math. 8, 36–40. https://doi.org/10.12962/J24775401. VSI2.7364.

Dickinson, C.F., Heal, G.R., 1999. Solid-liquid diffusion controlled rate equations. Thermochim. Acta 340–341, 89–103. https://doi.org/10.1016/s0040-6031(99)

Ekmekyapar, A., Aktaş, E., Künkül, A., Demirkiran, N., 2012. Investigation of leaching kinetics of copper from malachite ore in ammonium nitrate solutions. Metall. Mater. Trans. B Process Metall. Mater. Process. Sci. 43, 764–772. https://doi.org/10.1007/ S11663-012-9670-2/FIGURES/12.

Fazli, A., Rodrigue, D., 2020. Recycling waste tires into ground tire rubber (GTR)/rubber compounds: a review. J. Compos. Sci. 2020 4, 103. https://doi.org/10.3390/ JCS4030103, 4, 103.

Gregurek, D., Peng, Z., Wenzl, C., 2015. Lead and zinc metallurgy. JOM. https://doi.org/ 10.1007/s11837-015-1556-8.

- Gu, K., Li, W., Han, J., Liu, W., Qin, W., Cai, L., 2019. Arsenic removal from lead-zinc smelter ash by NaOH-H2O2 leaching. Sep. Purif. Technol. 209, 128–135. https:// doi.org/10.1016/J.SEPPUR.2018.07.023.
- Gunasekara, A.S., Donovan, J.A., Xing, B., 2000. Ground discarded tires remove naphthalene, toluene, and mercury from water. Chemosphere 41, 1155–1160. https://doi.org/10.1016/S0045-6535(00)00016-3.
- Gupta, V.K., Gupta, B., Rastogi, A., Agarwal, S., Nayak, A., 2011. Pesticides removal from waste water by activated carbon prepared from waste rubber tire. Water Res 45, 4047–4055. https://doi.org/10.1016/J.WATRES.2011.05.016.
- Gupta, V.K., Nayak, A., Agarwal, S., Tyagi, I., 2014. Potential of activated carbon from waste rubber tire for the adsorption of phenolics: effect of pre-treatment conditions. J. Colloid Interface Sci. 417, 420–430. https://doi.org/10.1016/J.JCIS.2013.11.067.
- Hörenz, C., Tache, O., Bartczack, D., Nunez, S., Alvaro, I.A., Goenaga-Infante, H., Hodoroaba, V.-.D., 2020. A study on the analysis of particle size distribution for bimodal model nanoparticles by electron microscopy. Microsc. Microanal. 26, 2282–2283. https://doi.org/10.1017/s1431927620021054.
- Huang, H., Tang, L., 2007. Treatment of organic waste using thermal plasma pyrolysis technology. Energy Convers. Manag. 48, 1331–1337. https://doi.org/10.1016/J. ENCONMAN 2006 08 013
- Huang, Y., Bird, R.N., Heidrich, O., 2007. A review of the use of recycled solid waste materials in asphalt pavements. Resour. Conserv. Recycl. 52, 58–73. https://doi.org/ 10.1016/J.RESCONREC.2007.02.002.
- Ippolito, N.M., Medici, F., Pietrelli, L., Piga, L., 2021. Effect of acid leaching pretreatment on gold extraction from printed circuit boards of spent mobile phones. Mater. 2021 14, 362. https://doi.org/10.3390/MA14020362, 14, 362.
- Isabell, T.C., Dravid, V.P., 1997. Resolution and sensitivity of electron backscattered diffraction in a cold field emission gun SEM. Ultramicroscopy 67, 59–68. https://doi. org/10.1016/S0304-3991(97)00003-X.
- Jing, L., Xu, Z., Sun, X., Shang, J., Cai, W., 2001. The surface properties and photocatalytic activities of ZnO ultrafine particles. Appl. Surf. Sci. 180, 308–314. https://doi.org/10.1016/S0160.4332(01)00365-8
- https://doi.org/10.1016/S0169-4332(01)00365-8.

 Johns, J., Rao, V., 2008. Characterization of natural rubber latex/chitosan blends. Int. J.
- Polym. Anal. Charact. 13, 280–291. https://doi.org/10.1080/10236660802190104. Kamegawa, K., Nishikubo, K., Yoshida, H., 1998. Oxidative degradation of carbon blacks with nitric acid (I) Changes in pore and crystallographic structures. Carbon N. Y. 36, 433–441. https://doi.org/10.1016/S0008-6223(97)00227-3.
- Karagöz, M., Ağbulut, Ü., Sandemir, S., 2020. Waste to energy: production of waste tire pyrolysis oil and comprehensive analysis of its usability in diesel engines. Fuel 275, 117844. https://doi.org/10.1016/J.FUEL.2020.117844.
- Kinoshita, T., Yamaguchi, K., Akita, S., Nii, S., Kawaizumi, F., Takahashi, K., 2005. Hydrometallurgical recovery of zinc from ashes of automobile tire wastes. Chemosphere 59, 1105–1111. https://doi.org/10.1016/j. chemosphere.2004.12.015.
- Kole, J.P., Löhr, A.J., Van Belleghem, F.G.A.J., Ragas, A.M.J., 2017. Wear and tear of tyres: a stealthy source of microplastics in the environment. Int. J. Environ. Res. Public Health 14. https://doi.org/10.3390/IJERPH14101265.
- Levenspiel, O., 1998. Chemical Reaction Engineering. Wiley.
- Liang, Y.C., Wang, C.C., 2018. Surface crystal feature-dependent photoactivity of ZnO–ZnS composite rods via hydrothermal sulfidation. RSC Adv. 8, 5063–5070. https://doi.org/10.1039/C7RA13061A.
- Lin, M., Liu, Y.Y., Lei, S.M., Ye, Z., Pei, Z.Y., Li, B., 2018. High-efficiency extraction of Al from coal-series kaolinite and its kinetics by calcination and pressure acid leaching. Appl. Clay Sci. 161, 215–224. https://doi.org/10.1016/J.CLAY.2018.04.031.
- Liu, X., Wang, J., Gheni, A., ElGawady, M.A., 2018. Reduced zinc leaching from scrap tire during pavement applications. Waste Manag. 81, 53–60. https://doi.org/ 10.1016/J.WASMAN.2018.09.045.
- Llompart, M., Sanchez-Prado, L., Pablo Lamas, J., Garcia-Jares, C., Roca, E., Dagnac, T., 2013. Hazardous organic chemicals in rubber recycled tire playgrounds and pavers. Chemosphere 90, 423–431. https://doi.org/10.1016/J. CHEMOSPHERE 2012 07 053
- Mazzoli, A., Favoni, O., 2012. Particle size, size distribution and morphological evaluation of airborne dust particles of diverse woods by Scanning Electron Microscopy and image processing program. Powder Technol. 225, 65–71. https:// doi.org/10.1016/J.POWTEC.2012.03.033.
- Mui, E.L.K., Ko, D.C.K., McKay, G., 2004. Production of active carbons from waste tyres—a review. Carbon N. Y. 42, 2789–2805. https://doi.org/10.1016/J. CARBON.2004.06.023.
- Nelson, S.M., Mueller, G., Hemphill, D.C., 1994. Identification of tire leachate toxicants and a risk assessment of water quality effects using tire reefs in canals. Bull. Environ. Contam. Toxicol. 52, 574.

- Nilsson, A.E., Aragonés, M.M., Torralvo, F.A., Dunon, V., Angel, H., Komnitsas, K., Willquist, K., 2017. A review of the carbon footprint of Cu and Zn production from primary and secondary sources. Minerals 7, 1–12. https://doi.org/10.3390/ pin/7090168
- Norwitz, G., Galan, M., 1967. Dissolution of carbon blacks by nitric acid. Carbon N. Y. 5, 287–289. https://doi.org/10.1016/0008-6223(67)90010-3.
- Rahimi, S.R., Nikbin, I.M., Allahyari, H., Habibi, T.S., 2016. Sustainable approach for recycling waste tire rubber and polyethylene terephthalate (PET) to produce green concrete with resistance against sulfuric acid attack. J. Clean. Prod. 126, 166–177. https://doi.org/10.1016/J.JCLEPRO.2016.03.074.
- Rhodes, E.P., Ren, Z., Mays, D.C., 2012. Zinc leaching from tire crumb rubber. Environ. Sci. Technol. 46, 12856–12863. https://doi.org/10.1021/ES3024379/SUPPL_FILE/FS3024379_SU01_PDF
- Seyed Ghasemi, S.M., Azizi, A., 2018. Alkaline leaching of lead and zinc by sodium hydroxide: kinetics modeling. J. Mater. Res. Technol. 7, 118–125. https://doi.org/ 10.1016/j.jmrt.2017.03.005.
- Sing, K.S.W., Everett, D.H., Haul, R.A.W., Moscou, L., Pierotti, R.A., Rouquerol, J., Siemieniewska, T., 1985. Reporting physisorption data for gas/solid systems with special reference to the determination of surface area and porosity. Pure Appl. Chem. 57, 603–619. https://doi.org/10.1351/pac198557040603.
- Singh, R., Varma, A.J., 2012. Towards biodegradable elastomers: green synthesis of carbohydrate functionalized styrene–butadiene–styrene copolymer by click chemistry. Green Chem. 14, 348–356. https://doi.org/10.1039/CIGC16146F.
- Sun, B., Li, J., Xiang, L., Lin, F., Che, L., Tian, W., Yan, B., Chen, G., 2022. Simulating vulcanization process during tire production to explore sulfur migration during pyrolysis. Fuel 330, 125665. https://doi.org/10.1016/J.FUEL.2022.125665.
- Tahir, M., Stöckelhuber, K.W., Mahmood, N., Komber, H., Formanek, P., Wießner, S., Heinrich, G., 2015. Highly reinforced blends of nitrile butadiene rubber and in-situ synthesized polyurethane–urea. Eur. Polym. J. 73, 75–87. https://doi.org/10.1016/ J.EURPOLYMJ.2015.09.024.
- Thaptong, P., Boonbumrung, A., Jittham, P., Sae-oui, P., 2019. Potential use of a novel composite zinc oxide as eco-friendly activator in Tire tread compound. J. Polym. Res. 26, 1–9. https://doi.org/10.1007/S10965-019-1895-1/TABLES/6.
- Thomas, B.S., Gupta, R.C., 2016. A comprehensive review on the applications of waste tire rubber in cement concrete. Renew. Sustain. Energy Rev. 54, 1323–1333. https://doi.org/10.1016/J.RSER.2015.10.092.
- Tran, T.Q., Skariah Thomas, B., Zhang, W., Ji, B., Li, S., Brand, A.S., 2022.
 A comprehensive review on treatment methods for end-of-life tire rubber used for rubberized cementitious materials. Constr. Build. Mater. 359, 129365 https://doi.org/10.1016/J.CONBUILDMAT.2022.129365.
- Tunc, M., Kocakerim, M.M., Küçük, Ö., Aluz, M., 2007. Dissolution of colemanite in (NH4)2SO4 solutions. Korean J. Chem. Eng. 2007 241 (24), 55–59. https://doi.org/ 10.1007/S11814-007-5009-0.
- Vladár, A.E., Hodoroaba, V.D., 2020. Characterization of nanoparticles by scanning electron microscopy. Charact. Nanoparticles Meas. Process. Nanoparticles 7–27. https://doi.org/10.1016/B978-0-12-814182-3.00002-X.
- Wadsworth Sec, M.E., Miller, J.D., 1979. Hydrometallurgical processes. Rate Process. Extr. Metall. 133–244. https://doi.org/10.1007/978-1-4684-9117-3_4.
- Wang, X., Zhou, L., Li, J., Han, N., Li, X., Liu, G., Jia, D., Ma, Z., Song, G., Zhu, X., Peng, Z., Zhang, L., 2021. The positive effect of ZnS in waste tire carbon as anode for lithium-ion batteries. Mater. 2021 14, 2178. https://doi.org/10.3390/MA14092178, 14. 2178.
- Wik, A., 2007. Toxic components leaching from tire rubber. Bull. Environ. Contam. Toxicol. 79, 114-119. https://doi.org/10.1007/S00128-007-9145-3/TABLES/2.
- Yamaguchi, K., Kinoshita, T., Akita, S., 2006. Thermal treatment of waste tire fly ash with polyvinyl chloride: selective leaching of zinc with water. Ind. Eng. Chem. Res. 45, 1211–1216. https://doi.org/10.1021/ie051118x.
- Yerezhep, D., Tychengulova, A., Sokolov, D., Aldiyarov, A., Multifaceted, A.A., Devasahayam, S., Singh, R., Strezov, V., 2021. A multifaceted approach for cryogenic waste tire recycling. Polym. 2021 13, 2494. https://doi.org/10.3390/ POLYM13152494, 13, 2494.
- Zhang, R., Ma, S., Yang, Q., Zheng, S., Zhang, Y., Kim, N., Hong, S., 2011. Research on NaCaHSiO4 decomposition in sodium hydroxide solution. Hydrometallurgy 108, 205–213. https://doi.org/10.1016/J.HYDROMET.2011.04.010.
- Zhang, X., Cao, H., Xie, Y., Ning, P., An, H., You, H., Nawaz, F., 2015. A closed-loop process for recycling LiNi1/3Co1/3Mn1/3O2 from the cathode scraps of lithium-ion batteries: process optimization and kinetics analysis. Sep. Purif. Technol. 150, 186–195. https://doi.org/10.1016/J.SEPPUR.2015.07.003.
- Zhou, D.J., Xie, X.Y., Zhang, Y.L., Guo, D.Y., Zhou, Y.J., Xie, J.F., 2016. Facile synthesis of ZnS nanorods in PEG and their spectral performance. Mater. Res. Express. 3, 105023 https://doi.org/10.1088/2053-1591/3/10/105023.